be ascribed to the stabilization experienced by an highly charged cation (Ni(III)) in an environment of increasing negative charge (due to the increase of ClO_4^- ions).

On increasing the $NaClO_4$ concentration, because of the opposite effects described above, the difference in stability of the Ni(III) complexes with [9]aneN$_3$ and cyclam, expressed by $\Delta E_{1/2}$, which is quite small at low $NaClO_4$ concentrations (0.1 M $NaClO_4$, $\Delta E_{1/2}$ = 25 mV), becomes larger and larger (7 M, 160 mV). Moreover for $NaClO_4$ concentrations greater than 3 M (see Figure 6), the $E_{1/2}$(Ni(III)/Ni(II)) value for the [16]aneN$_5$ complex becomes less positive than that of the cyclam analogue, thus inverting the previously established, apparently well-defined order.

Conclusions

This work has tried to throw light into the factors that control the attainment of the trivalent state of nickel polyamine complexes in solution. At this stage, the following conclusions can be drawn.

(1) The structural properties of the ligand (in particular the ring size) are a very selective element in the stabilization of Ni(III); this is particularly evident in the case of quadridentate macrocycles.

(2) Changing the solvent does not alter the relative trend of stability of Ni(III) complexes with different macrocycles: the nature of the solvent is not selective.

(3) In aqueous solutions the variation of the concentration of the so-called "inert" electrolyte introduces a novel element of selectivity, discriminating between redox changes involving or not involving water molecules.

Acknowledgment. Financial support of the Italian Ministry of Education (MPI; 40%) is gratefully acknowledged.

Contribution from the School of Chemical Sciences, University of Illinois, Urbana, Illinois 61801, Corporate Research Science Laboratories, Exxon Research and Engineering Company, Annandale, New Jersey 08801, and Department of Chemistry, Stanford University, Stanford, California 94305

Reactions of MoS_3, WS_3, WSe_3, and $NbSe_3$ with Lithium. Metal Cluster Rearrangement Revealed by EXAFS

Robert A. Scott,*[1a] Allan J. Jacobson,[1b] Russ R. Chianelli,[1b] W.-H. Pan,[1b] Edward I. Stiefel,[1b] Keith O. Hodgson,[1c] and Stephen P. Cramer*[1b]

Received July 31, 1985

EXAFS analysis has been used to study the structural changes that occur during the lithiation of the amorphous materials MoS_3, WS_3, and WSe_3 and the crystalline material $NbSe_3$. For the three amorphous materials, an increase in the number of metal–metal bonds was observed, as well as a significant decrease in the metal–metal distance. A reduction in the number of metal–chalcogenide interactions was also apparent, along with an increase in the metal–chalcogenide distance. For Li_4MoS_3, the predicted Mo–Mo and Mo–S distances are 2.66 (3) and 2.50 (3) Å, respectively. A reasonable model for this fully lithiated structure involves an octahedral Mo_6 cluster analogous to those found in Chevrel-phase materials. Similar clusters may be formed during lithiation of WS_3 and WSe_3. Predicted W–W and W–S distances were 2.64 (3) and 2.47 (3) Å for Li_4WS_3; for Li_5WSe_3, W–W and W–Se distances of 2.67 (3) and 2.61 (3) Å were found. In contrast with that of the amorphous trichalcogenides, lithiation of crystalline $NbSe_3$ results in a slight contraction of the average Nb–Se bond length. From Se EXAFS, it was found that a significant Se–Se interaction persists in this material after lithiation, and it is difficult to say whether or not significant metal cluster formation occurs. These results have implications for interpretation of the electrochemical behavior of these materials.

Introduction

The chemistry of molybdenum and tungsten combined with sulfur and selenium is extremely rich in its structural diversity and practical importance. The dichalcogenides (ME_2: M = Mo, W; E = S, Se) are well understood structurally, and are important for their catalytic and electrochemical properties.[2] The trichalcogenides (ME_3) are amorphous materials, which have been shown to react readily with *n*-butyllithium and alkali-metal naphthalides to form amorphous compositions such as M'_xMoS_3 (M' = Li, Na, K; $0 \le x \le 4$).[3] Electrochemically, MoS_3 cathodes in lithium cells show good reversibility provided they are not discharged further than the composition Li_3MoS_3.[4] The amorphous structure of these materials,[5] whether prepared by thermal or solution techniques,[6] has hindered their characterization. The Chevrel phases $M'_xMo_6E_8$ form a third clsss of molybdenum chalcogenides. These systems have been extensively studied because of their superconducting properties. Formally, the molybdenum oxidation state varies from +2 to $+2^2/_3$ depending on the value of x, overlapping that observed in the most reduced of the amorphous trichalcogenide compositions.

In a previous paper, EXAFS results on the untreated ME_3 materials were described.[7] Despite their lack of long-range order, local structure involving metal–metal bonding was observed, and a chainlike structure for MoS_3 was proposed.[8] This paper describes the dramatic structural changes that occur upon electrochemical lithiation of these materials. Clear evidence is found for the formation of higher order metal clusters, and a hexanuclear octahedral model is proposed for Li_4MoS_3. It thus appears that the amorphous trichalcogenides are important intermediates that can be transformed to dichalcogenides by heat or the Chevrel phase analogues electrochemically.

Experimental Section

Sample Preparation and Data Collection. The ME_3 starting materials were prepared by previously described methods from the $(NH_4)_2ME_4$ precursors.[7] Lithium was inserted into the trichalcogenides at ambient temperature either by electrochemical means or by reaction with *n*-butyllithium in dry hexane using published procedures.[3] Open-circuit voltages for 15 Li_xMoS_3 samples prepared by reaction with *n*-butyllithium were measured for comparison with the previous electrochemical

* To whom correspondence should be addressed.

(1) (a) University of Illinois. (b) Exxon Research and Engineering Co. (c) Stanford University.
(2) Chianelli, R. R. *Int. Rev. Phys. Chem.* **1982**, *2*, 127–165.
(3) Jacobson, A. J.; Chianelli, R. R.; Rich, S. M.; Whittingham, M. S. *Mater. Res. Bull.* **1979**, *14*, 1437–1448.
(4) Jacobson, A. J. *Solid State Ionics* **1981**, *5*, 65–70.
(5) Ratnasamy, P.; Rodrique, L.; Leonard, A. J. *J. Phys. Chem.* **1973**, *77*, 2242–2246.
(6) (a) Diemann, E.; Müller, A. *Coord. Chem. Rev.* **1973**, *10*, 79–122. (b) Chianelli, R. R.; Dines, M. B. *Inorg. Chem.* **1978**, *17*, 2758–2762.
(7) Cramer, S. P.; Liang, K. S.; Jacobson, A. J.; Chang, C. H.; Chianelli, R. R. *Inorg. Chem.* **1984**, *23*, 1215–1221.
(8) Liang, K. S.; de Neufville, J. P.; Jacobson, A. J.; Chianelli, R. R.; Betts, F. *J. Non-Cryst. Solids* **1980**, *35–36*, 1249–1254.

0020-1669/86/1325-1461$01.50/0

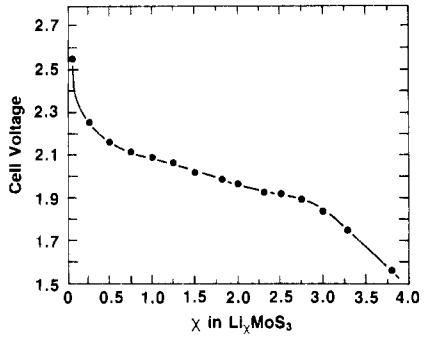

Figure 1. Resting potential of chemically lithiated MoS_3 samples as a function of degree of lithiation (see text for details).

data.[3,4] Samples of Li_xMoS_3 were formed into cathodes by loading the solids into stainless-steel-mesh bags, which were subsequently cold-pressed to ensure good electrical contacts. The cathodes were then immersed in a solution of $LiClO_4$ (1.6 M) in dioxolane and open-circuit voltages measured against a lithium foil cathode by using a high-impedance voltmeter. Cells were equilibrated for 1–3 days before voltages were recorded. All of the XAS spectra were recorded at the Stanford Synchrotron Radiation Laboratory in transmission mode with Si[220] or Si[111] crystal monochromators. Samples were shipped to Stanford in sealed tubes under an argon atmosphere and loaded into sample cells in a nitrogen-filled Vacuum Atmospheres glovebox. The sample cells were kept in a He-purged Lucite box with Kapton windows during data collection.

Data Manipulation and Analysis. The EXAFS was extracted from the absorption spectrum by previously described procedures,[9-11] smoothed by Gaussian convolution, and Fourier filtered. A curve-fitting analysis of the filtered data utilized the expression

$$\chi(k) = \sum_b \frac{N_b}{kR_{ab}^2} A_{ab}(k) [\exp(-2\sigma_{ab}^2 k^2)] \sin [2kR_{ab} + \alpha_{ab}(k)] \quad (1)$$

In this expression, N_b is the number of scatterers at distance R_{ab} with mean-square-distance deviation σ_{ab}^2. The total amplitude $A_{ab}(k)$ and phase shift $\alpha_{ab}(k)$ have been described previously.[7]

The phase shift functions were obtained from the ME_2 model compounds,[7] by parametrizing the phase shift as

$$\alpha_{ab}(k) = a_0 + a_1 k + a_2 k^m + a_3 k^n \quad (2)$$

and varying the parameters a_i to obtain the best possible fit to the data. No improvement was observed when the phase shift was obtained by using a complex Fourier back-transformation of single shells of EXAFS data.[12] In all cases, the same threshold energy (E_0) was used throughout the analysis.

The amplitude analysis for first coordination sphere interactions relied on tetrahedral ME_4^{2-} models whenever possible. The amplitude function was parametrized as

$$A(k) = c_0[\exp(c_1 k + c_2 k^2)]k^{c_3} \quad (3)$$

and the parameters c_i were varied to obtain the best fit. When this expression could not yield a good fit, as in the case of backscattering by tungsten in the first coordination sphere, the complex Fourier back-transform was used to extract a total amplitude envelope. In either case, the overall amplitude was corrected by calculating σ_{ab} from the vibrational frequencies.[10,11,13]

Frequently, it is not possible to find a model compound in which the σ_{ab} contribution is accurately known. In such cases, the results can be expressed as changes in σ_{ab} between model and unknown. Alternatively, one can adjust the empirical amplitude to yield the same σ_{ab} value derived by using the theoretical amplitude functions and a scale factor. This approach is similar to the FABM (fine adjustment based on models) procedure of Teo et al.[14] Both procedures have been used in the curve-fitting analysis of the lithiated trichalcogenides.

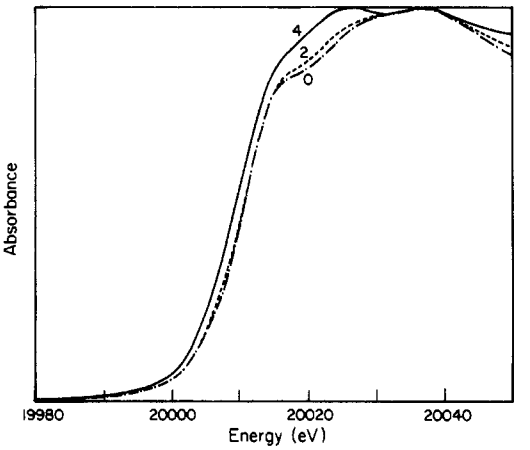

Figure 2. Molybdenum K-absorption edge changes in MoS_3 under various lithium loadings: untreated MoS_3 (-·-); Li_2MoS_3 (--); Li_4MoS_3 (—).

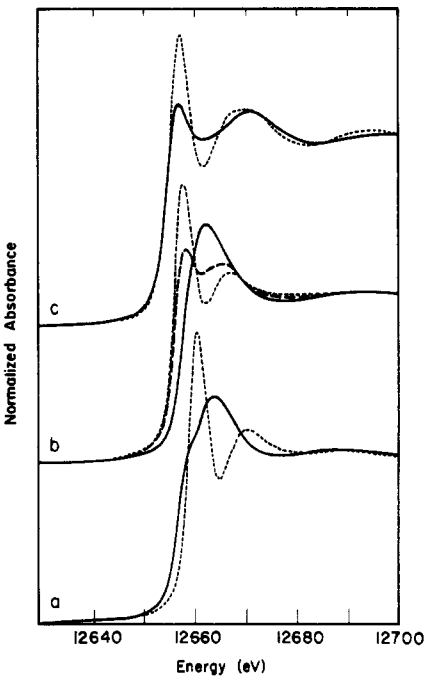

Figure 3. Selenium K-absorption edges: (a) untreated $NbSe_3$ (--), Li_3NbSe_3 (—); (b) untreated WSe_3 (--), Li_2WSe_3 (--), Li_5WSe_3 (—); (c) solid $Fe_2(Se_2)(CO)_6$ (--), $Li_2[Fe_2Se_2(CO)_6]$ in THF solution (—). The Fe_2Se_2 compounds were a kind gift from T. D. Weatherill and T. B. Rauchfuss and were prepared as described in ref 15.

Results

Oxidation State Changes upon Lithiation. The electrochemical insertion of lithium in MoS_3 under dynamic conditions has been reported previously.[3] Results under open-circuit conditions for the change in voltage as a function of composition for Li/Li_xMoS_3 ($0 \le x \le 4$) electrochemical cells are shown in Figure 1. The initial sharp drop in voltage to 2.1 V is followed by a smooth falloff to 1.86 V at the composition Li_3MoS_3. Beyond this point the voltage drops more rapidly to the limiting composition Li_4MoS_3. Similar behavior is observed under dynamic conditions, but the voltage profile is flatter and the falloff is more rapid beyond 3 Li per MoS_3. It has been observed that cells discharged beyond the composition Li_3MoS_3 do not recharge, indicating that an irreversible chemical change occurs in this composition region.

(9) Cramer, S. P.; Hodgson, K. O.; Stiefel, E. I.; Newton, W. E. *J. Am. Chem. Soc.* **1978**, *100*, 2748–2761.
(10) Cramer, S. P. In *EXAFS for Inorganic Systems*; Garner, C. D., Hasnain, S. S., Eds.; Daresbury Laboratory: Daresbury, U.K., 1981.
(11) Cramer, S. P.; Wahl, R.; Rajagopalan, K. V. *J. Am. Chem. Soc.* **1981**, *103*, 7721–7727.
(12) Eisenberger, P. M.; Shulman, R. G.; Kincaid, B. M.; Brown, G. S.; Ogawa, S. *Nature (London)* **1978**, *274*, 30–34.
(13) Cyvin, S. J. *Molecular Vibrations and Mean Square Amplitudes*; Elsevier: Amsterdam, 1968.
(14) Teo, B. K.; Antonio, M. R.; Averill, B. A. *J. Am. Chem. Soc.* **1983**, *105*, 3751–3762.

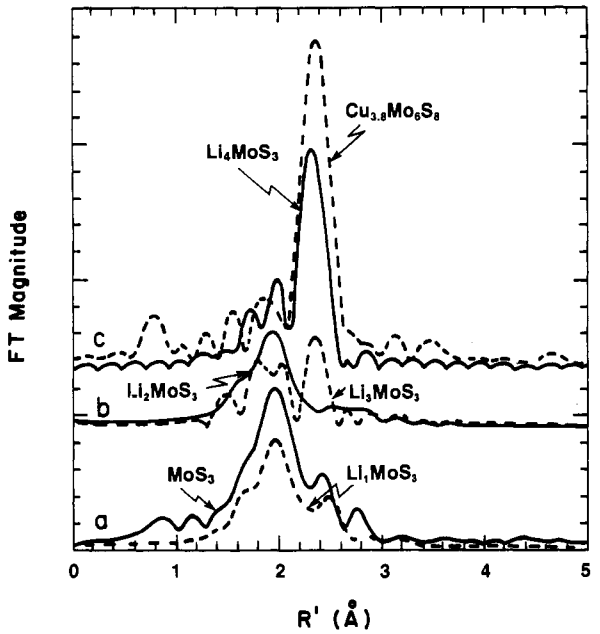

Figure 4. Mo EXAFS Fourier transforms (k = 4–18 Å^{-1}, k^3 weighting) for MoS_3 with progressively higher lithium loadings: (a) untreated MoS_3 (—), Li_1MoS_3 (--); (b) Li_2MoS_3 (—), Li_3MoS_3 (--); (c) Li_4MoS_3 (—), $Cu_{3.8}Mo_6S_8$ Chevrel phase (--).

The EXAFS results suggest that this irreversible change is to be associated with the formation of Mo–Mo-bonded metal clusters (vide infra).

Treatment of MoS_3 with lithium results in a progressive shift of the Mo edge to lower energies, as illustrated in Figure 2. This is consistent with the molybdenum becoming more reduced. Previously, it was proposed that, rather than $Mo^{VI}(S^{2-})_3$, a better formulation for MoS_3 would be $Mo^{V}_2(S_2^{2-})(S^{2-})_4$. From this formulation one would expect reduction of sulfur during lithiation. The fact that the molybdenum edge shifts more between Li_2MoS_3 and Li_4MoS_3 than between MoS_3 and Li_2MoS_3 may indicate that electrons initially reduce the disulfide bond preferentially.

In order to better understand the electronic changes associated with lithiation, the Se edges of WSe_3 and $NbSe_3$ were examined as a function of lithium loading. As illustrated in Figure 3, profound changes in the height and shape of the Se edge were observed. Addition of two lithiums to WSe_3 causes a significant decrease in the height of the main edge feature at 12 658 eV, with a concomitant increase in intensity around 12 665 eV. Virtually identical changes are observed in the Se edge spectra of $Fe_2(Se_2)(CO)_6$ upon reduction to $[Fe_2Se_2(CO)_6]^{2-}$ as shown in Figure 3c. The latter reaction is known to involve the breaking of the Se–Se bond in a diselenide bridge.[15] The Se edge spectra thus corroborate the suggestion that the initial reduction occurs at the dichalcogenide bond. Interpretation of the Se edge changes that occur upon conversion of Li_2WSe_3 to Li_5WSe_3 will have to await the study of other structurally characterized selenium compounds.

Structural Changes upon Lithiation. The Mo EXAFS Fourier transforms for MoS_3 with progressively higher lithium loadings are shown in Figure 4. Upon addition of a single lithium, the major change involves a decrease in the amplitude of the shorter distance Mo–S peak ($R' \cong 1.9$ Å). The feature at $R' \cong 2.4$ Å, associated with a short Mo–Mo interaction, decreases in intensity somewhat between MoS_3 and $LiMoS_3$, but is lost almost completely between $LiMoS_3$ and Li_2MoS_3. These results are again consistent with the idea that the disulfide bond is reduced first. Further lithiation causes dramatic increases in the amplitude of the short-distance Mo–Mo feature in Li_3MoS_3 and in Li_4MoS_3. It is clear that a significant structural rearrangement takes place during this part of the reaction of lithium with this material,

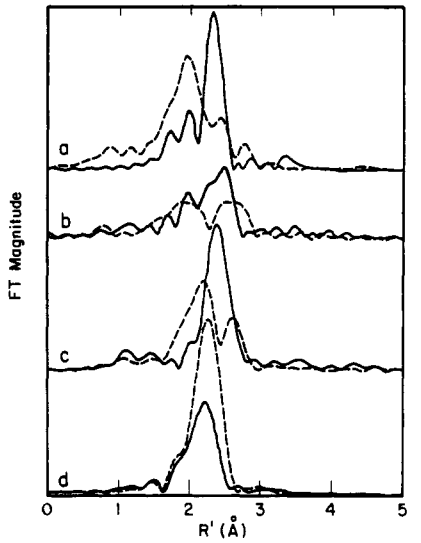

Figure 5. M EXAFS Fourier transforms (k^3 weighting, k = 4–18 Å^{-1}; except for WS_3 k = 4–16 Å^{-1}) for ME_3 materials before and after maximum lithiation: (a) untreated MoS_3 (--), Li_4MoS_3 (—); (b) untreated WS_3 (--), Li_4WS_3 (—); (c) untreated WSe_3 (--), Li_5WSe_3 (—); (d) untreated $NbSe_3$ (--), Li_3NbSe_3 (—).

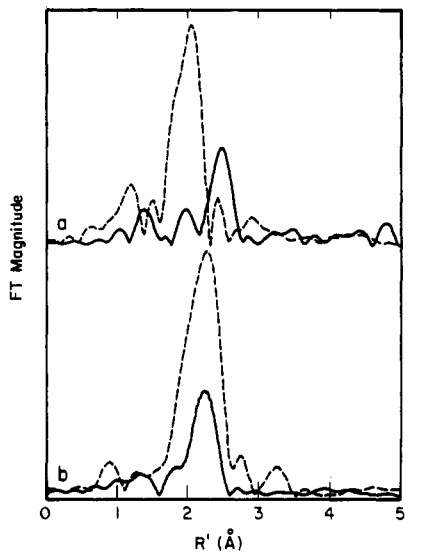

Figure 6. Se EXAFS Fourier transforms (k^3 weighting, k = 4.0–16.0 Å^{-1}) for lithiated materials: (a) untreated WSe_3 (--), Li_5WSe_3 (—); (b) untreated $NbSe_3$ (--), Li_3NbSe_3 (—).

resulting in fewer or more disordered Mo–S interactions and a greater number of short ($R' \cong 2.4$ Å) Mo–Mo interactions.

Similar structural rearrangements take place in WS_3 and WSe_3, as illustrated in Figure 5. In contrast, the crystalline material $NbSe_3$, which is also electrochemically active, exhibited a smaller Nb–Se transform peak upon uptake of three lithiums. This may indicate a decreased or more disordered Nb–Se interaction, but it might also arise from destructive interference by a Nb–Nb interaction.[16] It was also possible to observe changes by using the Se EXAFS of WSe_3 and $NbSe_3$, and the Fourier transforms are shown in Figure 6. The tungsten triselenide data clearly indicate a longer Se–W interaction, whereas the $NbSe_3$ EXAFS shows only a diminished Se–Nb interaction upon lithiation.

In order to obtain a more quantitative interpretation of the structural changes associated with lithiation, curve-fitting analysis was required. In this analysis, three different variables *had* to

(15) Weatherill, T. D.; Rauchfuss, T. B.; Scott, R. A. *Inorg. Chem.*, following paper in this issue.

(16) Other examples of coincidental destructive interference of EXAFS from different shells of scatterers have been documented. For example, see: Antonio, M. R.; Teo, B. K.; Averill, B. A. *J. Am. Chem. Soc.* **1985**, *107*, 3583–3590.

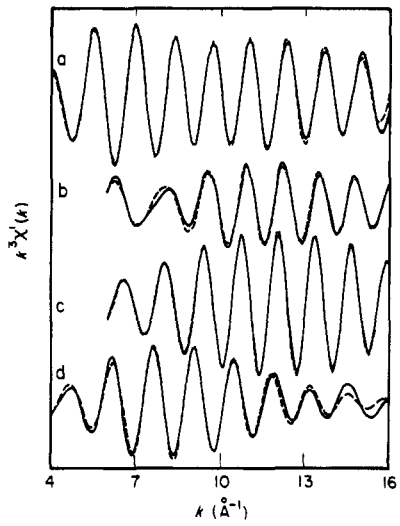

Figure 7. Curve-fitting analysis of fully lithiated ME_3 materials using M EXAFS, showing filtered data (—) and fit (--): (a) Li_4MoS_3; (b) Li_4WS_3; (c) Li_5WSe_3, (d) Li_3NbSe_3.

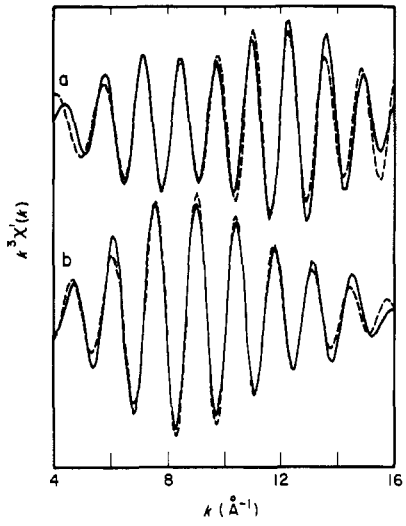

Figure 8. Curve-fitting analysis of fully lithiated MSe_3 materials using Se EXAFS showing filtered data (—) and fit (--): (a) Li_5WSe_3; (b) Li_3NbSe_3.

be adjusted: the coordination number N_b, the Debye-Waller factor $\exp(-2\sigma_{ab}^2k^2)$, and the interatomic distance R_{ab}. The close correlation between N_b and σ_{ab} can cause large errors when both are adjusted simultaneously. On the other hand, dramatic changes in σ_{ab} have been observed during cluster transformations,[17] so use of a fixed σ_{ab} cannot be justified. To test the stability of such a fitting procedure, the previously reported EXAFS spectra of several metal–sulfur clusters were reanalyzed according to the new procedures. The results for the ME_3 starting materials and their lithiated analogues are summarized in Table I.

Table II (supplementary material) contains the curve-fitting results on several structurally characterized model compounds. Although the distances were calculated with high accuracy, the metal–metal coordination numbers were sometimes in error by as much as +40% to −28%. These errors were not correlated with the type of amplitude function used; rather, they are intrinsic to the crude treatment of multiple-scattering effects. Hence, for structure predictions, it is necessary to use an error of ±50% for the second-shell coordination numbers. First-shell errors are more likely ±25%. Representative fits of the EXAFS of fully lithiated samples are illustrated in Figures 7 and 8. The numerical results for the lithiated samples are compared with revised analyses of the untreated ME_3 data in Table I.

Chart I

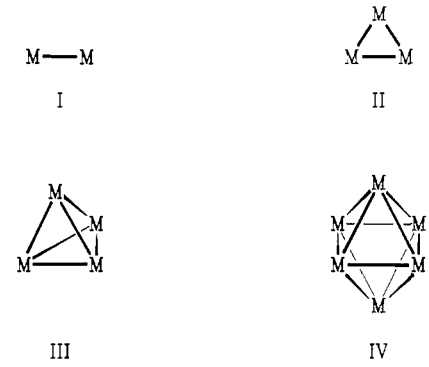

The MoS_3 curve-fitting results quantitate the drastic changes revealed in the Fourier transforms. The closest Mo–Mo interaction shortened by nearly 0.1 Å, from 2.75 to 2.66 Å. Meanwhile, the average Mo–S bond lengthened from 2.41 to 2.50 Å. The coordination number changes are less precise, but the number of Mo–Mo interactions clearly increases while the average number of Mo–S bonds diminishes from ~6 to 3 or 4.

Similar results were obtained when the EXAFS spectra of lithiated WS_3 and WSe_3 were examined. Fully lithiated WS_3 showed a 0.11-Å contraction in the W–W distance and an increase in the W–W amplitude. The W–S bond increased from 2.38 to 2.47 Å. Upon full lithiation of WSe_3, a 0.1-Å reduction in the W–W distance and a 0.06-Å lengthening of the W–Se bond were observed. However, the changes in coordination number were ambiguous. Contributing to this uncertainty is the fact that the W–Se and W–W distances have moved within 0.05 Å of each other, so that the values obtained for the two shells are closely correlated. The Se EXAFS of fully lithiated WSe_3 confirmed this elongation of the Se–W distances and the decrease in the average number of Se–W interactions.

It is difficult to deduce the structural changes occurring during $NbSe_3$ lithiation, since no new transform features appear. However, it is clear that this crystalline material behaved differently from the amorphous materials. No dramatic lengthening of the Nb–Se distance was observed. If anything, there was a 0.02-Å contraction to 2.66 Å. Fitting the Se EXAFS yielded a Se–Nb distance of 2.62 Å, as well as a Se–Se interaction at 2.39 Å with a very large Debye–Waller factor.

Discussion

The EXAFS results on fully lithiated MoS_3, WS_3, and WSe_3 are consistent with an increase in the size of the metal clusters present in these materials. It is useful to consider some of the structures of species that may be involved and the bonding that may occur (Chart I).

For the Mo–S system, examples of isolated discrete clusters are available for all four structural types. As the oxidation state of the molybdenum is lowered, the number of d electrons available for metal–metal bonding increases. Hence, the strength of the metal–metal interaction can increase via multiple bonding, or the size of the metal cluster can increase.

An example of a simple dinuclear species as in I is the Mo(V) dimer $[(S_2)_2Mo(S_2)_2Mo(S_2)_2]^{2-}$, which has a Mo–Mo distance of 2.83 Å and a pair of disulfide bridges.[18] A representative trinuclear species is the Mo(IV) trimer $[Mo_3(S)(S_2)_6]^{2-}$, which has a triangular Mo_3 core with 2.72-Å Mo–Mo bond lengths, a capping S^{2-} ion, and three bridging S_2^{2-} ions.[19] Regular tetranuclear species are not common, but a recent example is the Mo(III) cluster $[Mo_4S_4(CN)_{12}]^{8-}$, which has a cubane-like Mo_4S_4 core and an average Mo–Mo distance of 2.85 Å.[20] Finally,

(17) Cramer, S. P.; Eidem, P. K.; Dori, Z.; Gray, H. B. *J. Am. Chem. Soc.* **1983**, *105*, 799–802.

(18) Müller, A.; Nolte, W. O.; Krebs, B. *Angew. Chem., Int. Ed. Engl.* **1978**, *17*, 279.

(19) Müller, A.; Pohl, S.; Dartmann, M.; Cohen, J. P.; Bennett, J. M.; Kirchner, R. M. *Z. Naturforsch., B: Anorg. Chem., Org. Chem.* **1979**, *34b*, 434–436.

Table I. Curve-Fitting Results for Lithiated Trichalcogenides

				A–B interaction				A–A interaction				
material	A–B[a]	anal.[b]	fit range, $Å^{-1}$	N_b	scale factor[c]	R, Å	σ, Å	N_b	scale factor[c]	R, Å	σ, Å	F[d]
MoS_3	Mo–S	emp	4–16	5.7	1.00	2.42	0.083	2.3	0.68	2.75	0.074	0.280
		emp	4–20	5.3	1.00	2.41	0.080	1.2	0.67	2.75	0.050	0.345
		theor	4–16	5.3	1.00	2.42	0.080	1.8	0.37	2.75	0.065	0.289
Li_4MoS_3	Mo–S	emp	4–16	3.1	1.00	2.50	0.078	4.1	0.68	2.66	0.056	0.309
		emp	4–20	2.8	1.00	2.49	0.072	4.2	0.67	2.66	0.055	0.550
		theor	4–16	3.5	1.00	2.51	0.084	3.4	0.37	2.66	0.058	0.360
WS_3	W–S	emp	6–16	6.2	1.00	2.38	0.133	2.6	0.95	2.75	0.064	0.257
		theor	6–16	6.0	1.00	2.38	0.136	2.1	0.24	2.75	0.060	0.291
Li_4WS_3	W–S	emp	6–16	3.2	1.00	2.47	0.087	3.6	0.95	2.64	0.067	0.294
		theor	6–16	3.3	1.00	2.47	0.084	3.0	0.24	2.64	0.064	0.299
WSe_3	W–Se	emp	6–16	9.4	1.00	2.55	0.112	0.94	1.36	2.77	0.041	0.332
		theor	6–16	8.5	1.00	2.55	0.110	1.57	0.27	2.77	0.056	0.404
	Se–W	array	4–16	0.76	1.00	2.58	0.092	1.75	1.00	2.37	0.078	0.233
		theor[f]	4–16	0.91	0.63	2.58	0.095	1.73	0.56	2.37	0.079	0.213
Li_5WSe_3	W–Se	emp	6–16	1.8	1.00	2.61	0.059	1.07	1.36	2.67	0.027	0.168
		theor	6–16	1.2	1.00	2.60	0.027	0.47	0.27	2.70	*e*	0.257
	Se–W	array	4–16	0.91	1.00	2.61	0.076					0.191
		theor[f]	4–16	0.81	0.63	2.61	0.073					0.201
$NbSe_3$	Nb–Se	emp	4–16	6.9	1.00	2.68	0.081					0.487
		theor	4–16	7.0	0.51	2.68	0.082					0.470
		diff[g]	...	8	...	2.68	...					...
	Se–Nb	emp	4–16	2.2	1.00	2.65	0.070	1.1	1.00	2.37	0.079	0.339
		theor[f]	4–16	2.1	0.38	2.65	0.070	1.4	0.56	2.37	0.083	0.318
		diff[g]	...	2[h]	...	2.65	...	1	...	2.37	...	...
Li_3NbSe_3	Nb–Se	emp	4–16	4.7	1.00	2.66	0.089					0.404
		theor	4–16	4.6	0.51	2.66	0.090					0.411
	Se–Nb	emp	4–16	1.6	1.00	2.62	0.087	0.64	1.00	2.39	0.116	0.153
		theor[f]	4–16	1.6	0.38	2.62	0.084	1.4	0.56	2.39	0.136	0.124

[a] EXAFS was performed with element A as the absorber. B is the backscatterer for which the curve-fitting was performed. [b] Analytical technique: diff, X-ray diffraction results; emp, parametrized empirical amplitude and phase functions used for EXAFS curve-fitting (model compounds used MoS_2 (Mo–S), WS_2 (W–S), WSe_2 (W–Se), $NbSe_2$ (Nb–Se), $NbSe_2$ (Se–Nb), MoS_2 (Mo–Mo), WS_2 (W–W), $NbSe_2$ (Nb–Nb), Se^0 (Se–Se); fitting results for these and other structurally characterized compounds given in Table II, available as supplementary material); theor, theoretical amplitude and phase functions used for A–A interaction only; array, amplitude and phase functions derived from complex back-transformation using $[WSe_4]^{2-}$ Se EXAFS. [c] The theoretical scale factor is the average ratio between the observed EXAFS amplitude and the theoretical electron–atom backscattering amplitude $f(\pi,k)$ from the tables of Teo et al.[14] The empirical scale factor is the correction to the empirical amplitude function reported in ref 7, required because of a different fitting range or different intervening atom. [d] The function value (F) is the sum of squared differences between best fit and actual EXAFS given by

$$F = [\sum_{i=1}^{N}[k^3(\chi^i_{calcd} - \chi^i_{obsd})]^2/(N-1)]^{1/2}$$

[e] Calculated $\sigma^2 = 0.0006$ Å^2, obviously not a physically correct result. [f] Theoretical amplitude used for A–B interaction also. [g] Reference 26. [h] This number does not include interchain Se–Nb interactions (see ref 26).

molecular examples of Mo–S systems with octahedral hexanuclear species such as IV are not yet known. However, the well-known Mo(II) cluster $[Mo_6Cl_8]^{4+}$ has the requisite Mo_6 core.[21] Of more relevance, there is a well-developed solid-state chemistry of "Chevrel-phase" compounds of the formula $M'_xMo_6E_8$. The basic structural unit of the Chevrel phases can be described as an octahedron of molybdenums, with each octahedral face capped by a chalcogenide. One of the most symmetric Chevrel-phase compounds, $Cu_{3.66}Mo_6S_8$, has an average Mo–Mo distance of 2.67 Å,[22] similar to the Li_4MoS_3 Mo–Mo distance of 2.66 Å. It is possible that a similar core structure exists in both materials.

Hughbanks and Hoffmann have reported a combined molecular orbital and crystal orbital analysis of systems containing $Mo_{3n}E_{3n+2}$ units.[23] They view the Mo_6E_8 units as "built from two Mo_3E_3 planar fragments, staggered and stacked one upon the other, then capped top and bottom by chalcogenides." This fragment approach, although perhaps originally intended only for computational purposes, may actually have relevance for the structural changes that occur during lithiation. It is interesting to speculate on the mechanism of the transformation of MoE_3 into Mo_6E_8 (or similar) clusters. Since the amorphous ME_3 materials are proposed to have a chain structure,[8] condensation into higher nu-

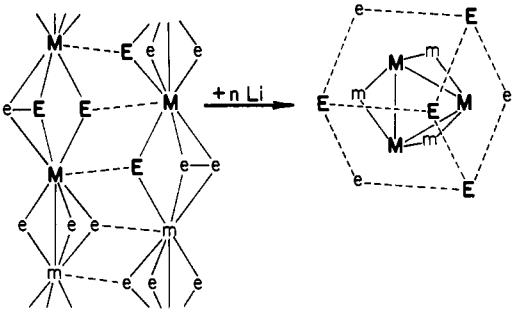

Figure 9. Plausible structural rearrangement upon incorporation of lithium into the amorphous ME_3 materials. The structure on the left represents the proposed chain structure for MoS_3.[8] The result of lithiation is the formation of high-nuclearity clusters as exemplified by the Chevrel phase structure on the right. Upper case letters are used to suggest a possible aggregation of M atoms from neighboring ME_3 chains.

(20) Müller, A.; Eltzner, W.; Bögge, H.; Jostes, R. *Angew. Chem., Int. Ed. Engl.* **1982**, *21*, 795–796.
(21) Vaughan, P. A. *Proc. Natl. Acad. Sci. U.S.A.* **1950**, *36*, 461–464.
(22) Yvon, K.; Paoli, A.; Flükiger, R.; Chevrel, R. *Acta Crystallogr., Sect B: Struct. Crystallogr. Cryst. Chem.* **1977**, *B33*, 3066–3072.
(23) Hughbanks, T.; Hoffmann, R. *J. Am. Chem. Soc.* **1983**, *105*, 1150–1162.
(24) Marezio, M.; Dernier, P. D.; Menth, A.; Hull, G. W., Jr. *J. Solid State Chem.* **1972**, *4*, 425–429.
(25) Pearson, W. B. *Handbook of Lattice Spacings and Structures of Metals*; Pergamon: New York, 1967; Vol. 2, p 88.
(26) Hodeau, J. L.; Marezio, M.; Roucau, C.; Ayroles, R.; Meerschaut, A.; Rouxel, J.; Monceau, P. *J. Phys. C* **1978**, *11*, 4117–4134.

clearity clusters most probably involves interchain interactions. A plausible transformation is illustrated in Figure 9. Here, a M_3E_4 unit (half of M_6E_8) is built up from two metals in one chain and one metal in a neighboring chain. The chalcogenide that bridged the two chains in ME_3 becomes the "cap" of the M_3E_4 unit. The other half of the M_6E_8 cluster can be imagined to be contributed by another layer of interacting ME_3 chains. Of course, the EXAFS alone can shed no light on the nature of the intermediate structures involved in such a transformation. Perhaps other experiments could better address this point.

Summary

EXAFS analysis has shown that lithiation of the amorphous materials MoS_3, WS_3, and WSe_3 results in a condensation into larger metal cluster, which may be similar to the clusters found in Chevrel-phase structures. This result is consistent with chemical trends previously observed in molecular cluster chemistry. These lithiated materials represent a unique transition region between small molecular clusters and the solid state, and they may be of synthetic value in the creation of large metal-chalcogenide clusters.

Acknowledgment. The X-ray absorption measurements were performed at the Stanford Synchrotron Radiation Laboratory (SSRL), which is supported by the Department of Energy, Office of Basic Energy Sciences. The work was performed while R.A.S. was at Stanford as a NIH Postdoctoral Fellow. XAS work under K.O.H. is supported by the NSF and NIH.

Registry No. MoS_3, 12033-29-3; WS_3, 12125-19-8; WSe_3, 88981-34-4; $NbSe_3$, 12034-78-5; Li_4MoS_3, 76770-55-3; Li_4WS_3, 101011-07-8; Li_5WSe_3, 101011-08-9; Li_3NbSe_3, 55886-04-9; MoS_2, 1317-33-5; $[Mo_2(S_2)_6]^{2-}$, 97278-58-5; $[Mo_3(S)(S_2)_6]^{2-}$, 88765-92-8; WS_2, 12138-09-9; WSe_2, 12067-46-8; $[WSe_4]^{2-}$, 21559-01-3; $NbSe_2$, 12034-77-4; Se, 7782-49-2; $[Fe_2Se_2(CO)_6]^{2-}$, 101011-09-0; $Fe_2Se_2(CO)_6$, 76185-26-7; Li, 7439-93-2; $LiMoS_3$, 101011-10-3; Li_2MoS_3, 101011-11-4; Li_3MoS_3, 101011-12-5.

Supplementary Material Available: Table II, containing reanalysis of curve fitting for the structurally characterized compounds MoS_2, $[Mo_2(S_2)_6]^{2-}$, $[Mo_3(S)(S_2)_6]^{2-}$, WS_2, WSe_2, $[WSe_4]^{2-}$, $NbSe_2$, and Se^0 (3 pages). Ordering information is given on any current masthead page.

Contribution from the School of Chemical Sciences, University of Illinois, Urbana, Illinois 61801

Structural Evidence Concerning the Frontier Orbitals in $[Fe_2E_2(CO)_6]^{2-}$ (E = S, Se): Redox-Active Dichalcogen Ligands

Timothy D. Weatherill, Thomas B. Rauchfuss,* and Robert A. Scott*

Received October 18, 1985

Fe and Se extended X-ray absorption fine structure (EXAFS) data have been used to determine the structures of the Fe_2E_2 (E = S, Se) cores of the following compounds: $[Fe_2E_2(CO)_6]^z$ (z = 0, 2-), $Fe_2(\mu\text{-}ER)_2(CO)_6$ (R = alkyl), $[Fe_2E_2(NO)_4]^{2-}$, and $Fe_2(\mu\text{-}ER)_2(NO)_4$. For the carbonyl compounds, the Fe EXAFS results indicate that the Fe–C, Fe–Fe, and Fe–E distances change little upon conversion of $Fe_2(E_2)(CO)_6$ to $[Fe_2E_2(CO)_6]^{2-}$ and $Fe_2(\mu\text{-}ER)_2(CO)_6$. The Se EXAFS results are consistent with the Fe EXAFS data, also showing that the two-electron reduction of $Fe_2(Se_2)(CO)_6$ results in breaking of the Se–Se bond. The Fe and Se EXAFS of the related nitrosyls $[Fe_2E_2(NO)_4]^{2-}$ and $Fe_2(\mu\text{-}ER)_2(NO)_4$ confirm that the Fe_2E_2 cores of these complexes are similar. All of the EXAFS results are consistent with the LUMO of $Fe_2(E_2)(CO)_6$, being mainly E–E antibonding in character.

Introduction

Since its preparation in the mid-1950s,[1] the compound $Fe_2(S_2)(CO)_6$ has been the subject of a number of investigations. Its solid-state structure as determined by Wei and Dahl features a tetrahedral Fe_2S_2 core, acute Fe–S–Fe angles, and a short Fe–Fe distance of 2.55 Å.[2] On the basis of this data, all atoms within the Fe_2S_2 core are considered to be mutually bonded. Several theoretical studies have dealt with the bonding and electronic structure of this species, the nature of the Fe–Fe bond being the primary focus.[3,4] Wei and Dahl suggested that the structure of $Fe_2(S_2)(CO)_6$ is due in part to the presence of a "bent" Fe–Fe bond. The origin of the iron orbitals responsible for this bond may be found by considering each iron atom as being octahedrally coordinated, the Fe–Fe bond arising from orbitals occupying the (sixth) position trans to the axial carbonyl ligands. Teo et al. supported this interpretation with a Fenske–Hall calculation and assigned the HOMO and LUMO to the bonding and antibonding components of the Fe–Fe interaction.[4] An ab initio calculation also describes the Fe–Fe interaction in terms of a "bent" bond and assigns this molecular orbital as the HOMO.[5] Self-consistent-field Xα scattered-wave molecular orbital calculations done by Andersen et al., provide a modified picture of the bonding situation in $Fe_2(S_2)(CO)_6$.[6] The SCF-Xα-SW results, together with a He I photoelectron study, indicate that the S_2 bridge enhances and stabilizes the π-component of the Fe–Fe bond. The assertion by Andersen et al. that the Fe–Fe bond possesses some multiple-bond character has been disputed by DeKock and co-workers on the basis of He I and He II photoelectron spectroscopy and Hartree–Fock–Slater calculations.[7] They argue that the LUMO in $Fe_2(S_2)(CO)_6$ is antibonding with respect to the sulfur atoms, not the iron atoms.

The chemistry of the dianion $[Fe_2S_2(CO)_6]^{2-}$ suggests that the LUMO in $Fe_2(S_2)(CO)_6$ is indeed primarily S–S antibonding.[8] Thus, Seyferth and co-workers have demonstrated that the reactivity of $[Fe_2S_2(CO)_6]^{2-}$ is sulfur-localized. Alkylation and metalation of this dianion afford neutral $Fe_2(\mu\text{-}SR)_2(CO)_6$ derivatives: the integrity of the Fe–Fe bond is retained in the products (eq 1).

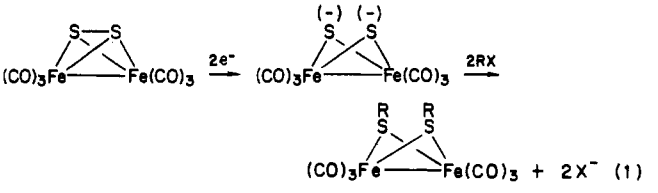

(1)

Although the structures of these alkylated and metalated products are firmly established, the structure of the parent dianion remains unknown. Herein we report the determination of the

(1) Hieber, W.; Gruber, J. *Z. Anorg. Allg. Chem.* **1958**, *296*, 91.
(2) Wei, C. H.; Dahl, L. F. *Inorg. Chem.* **1965**, *4*, 493. Wei, C. H.; Dahl, L. F. *Inorg. Chem.* **1965**, *4*, 1.
(3) For related theoretical discussions see: Burdett, J. K. *J. Chem. Soc., Dalton Trans.* **1977**, 423. Summerville, R. H.; Hoffmann, R. *J. Am. Chem. Soc.* **1976**, *98*, 7240. Mason, R.; Mingos, D. M. P. *J. Organomet. Chem.* **1973**, *50*, 53. Teo, B. K.; Hall, M. B.; Fenske, R. G.; Dahl, L. F. *J. Organomet. Chem.* **1974**, *70*, 413.
(4) Teo, B. K.; Hall, M. B.; Fenske, R. F.; Dahl, L. F. *Inorg. Chem.* **1975**, *14*, 3103.
(5) Van Dam, H.; Louwen, J. N.; Oskam, A.; Doran, M.; Hillier, I. H. *J. Electron Spectrosc. Relat. Phenom.* **1980**, *21*, 57.
(6) Andersen, E. L.; Fehlner, T. P.; Foti, A. E.; Salahub, D. R. *J. Am. Chem. Soc.* **1980**, *102*, 7422.
(7) DeKock, R. L.; Baerends, E. J; Hengelmolen, R. *Organometallics* **1984**, *3*, 289. DeKock, R. L.; Baerends, E. J.; Hengelmolen, R. *Inorg. Chem.* **1983**, *22*, 4158.
(8) Seyferth, D.; Henderson, R. S. *Organometallics* **1982**, *1*, 125.

0020-1669/86/1325-1466$01.50/0